Received: 27 March 2020 | Revised: 3 May 2020 | Accepted: 18 May 2020

DOI: 10.1002/ijc.33137

IJC International Journal of Cancer

CANCER THERAPY AND PREVENTION

Characterization of a dual BET/HDAC inhibitor for treatment of pancreatic ductal adenocarcinoma

Xin Zhang[1,2] | Tim Zegar[1,2] | Tim Weiser[3,4,5] | Feda H. Hamdan[6,7] | Benedict-Tilman Berger[3,4] | Romain Lucas[3,4,5] | Dimitrios-Ilias Balourdas[3,4] | Swetlana Ladigan[8,9] | Phyllis F. Cheung[1,2] | Sven-Thorsten Liffers[1,2] | Marija Trajkovic-Arsic[1,2] | Bjoern Scheffler[10] | Andreas C. Joerger[3,4,5] | Stephan A. Hahn[8] | Steven A. Johnsen[6,7] | Stefan Knapp[3,4,5] | Jens T. Siveke[1,2]

[1]Institute for Developmental Cancer Therapeutics, West German Cancer Center, University Medicine Essen, Essen, Germany

[2]Division of Solid Tumor Translational Oncology, German Cancer Consortium (DKTK, partner site University Hospital Essen) and German Cancer Research Center, DKFZ, Heidelberg, Germany

[3]Structural Genomics Consortium, Buchmann Institute for Life Sciences, Goethe University Frankfurt, Frankfurt, Germany

[4]Institute of Pharmaceutical Chemistry, Goethe University Frankfurt, Frankfurt, Germany

[5]German Cancer Network (DKTK), Frankfurt, Germany

[6]Department of General, Visceral and Pediatric Surgery, University Medical Center Göttingen, Göttingen, Germany

[7]Gene Regulatory Mechanisms and Molecular Epigenetics Lab, Division of Gastroenterology and Hepatology, Mayo Clinic, Rochester, Minnesota

[8]Department of Molecular Gastrointestinal Oncology, Ruhr-University Bochum, Bochum, Germany

[9]Department of Internal Medicine, Knappschaftskrankenhaus Bochum, Ruhr-University of Bochum, Bochum, Germany

[10]DKFZ Division of Translational Neurooncology, West German Cancer Center, DKTK partner site University Hospital Essen, Essen, Germany

Correspondence
Stefan Knapp, Buchmann Institute for Molecular Life Sciences and Institute of Pharmaceutical Chemistry, Goethe University Frankfurt, Max-von-Laue-Str. 9, 60438 Frankfurt am Main, Germany.
Email: knapp@pharmchem.uni-frankfurt.de

Jens T. Siveke, Institute for Developmental Cancer Therapeutics and Division of Solid Tumor Translational Oncology (German Cancer Consortium (DKTK), partner site Essen), West German Cancer Center, University Hospital Essen, Hufelandstraße 55, Essen D-45147, Germany.
Email: jens.siveke@uk-essen.de

Funding information
Deutsche Forschungsgemeinschaft, Grant/Award Numbers: Clinical Research Unit KFO337 / SI1549/3-1, SFB824 (project C4)

Abstract

Pancreatic ductal adenocarcinoma (PDAC) is resistant to virtually all chemo- and targeted therapeutic approaches. Epigenetic regulators represent a novel class of drug targets. Among them, BET and HDAC proteins are central regulators of chromatin structure and transcription, and preclinical evidence suggests effectiveness of combined BET and HDAC inhibition in PDAC. Here, we describe that TW9, a newly generated adduct of the BET inhibitor (+)-JQ1 and class I HDAC inhibitor CI994, is a potent dual inhibitor simultaneously targeting BET and HDAC proteins. TW9 has a similar affinity to BRD4 bromodomains as (+)-JQ1 and shares a conserved binding mode, but is significantly more active in inhibiting HDAC1 compared to the parental HDAC inhibitor CI994. TW9 was more potent in inhibiting tumor cell proliferation compared to (+)-JQ1, CI994 alone or combined treatment of both inhibitors. Sequential administration of gemcitabine and TW9 showed additional synergistic antitumor effects. Microarray analysis revealed that dysregulation of a FOSL1-directed transcriptional program contributed to the antitumor effects of TW9. Our

Abbreviations: BET, bromodomain and extra-terminal; DNMT, DNA methyltransferase; HDAC, histone deacetylase; NMC, NUT midline carcinoma; PDAC, pancreatic ductal adenocarcinoma; SE, super-enhancer.

Xin Zhang, Tim Zegar and Tim Weiser shared equally to the first authorship.

and JO1473/1-1; Deutsche Krebshilfe, Grant/Award Number: PIPAC consortium/grant no. 70112505; Deutsches Konsortium für Translationale Krebsforschung, Grant/Award Numbers: JF MYC, SGC/ charity no. 1097737

results demonstrate the potential of a dual chromatin-targeting strategy in the treatment of PDAC and provide a rationale for further development of multitarget inhibitors.

KEYWORDS

BET inhibitor, combined therapy, dual BET/HDAC inhibitor, HDAC inhibitor, pancreatic ductal adenocarcinoma

1 | INTRODUCTION

Tumorigenesis is often considered a consequence of the accumulation of driver mutations. However, the extensive intratumor and intertumor heterogeneity in established tumors involves additional regulatory layers controlling transcriptomic activity. The epigenome, a key determinant of the transcriptional output, controls cell identity and disease status. In contrast to the irreversibility of genomic mutations, aberrant epigenomic changes can potentially be reversed by small molecules targeting chromatin modulators. Epigenome-targeting drugs that are approved or in clinical trials include DNA methyltransferase inhibitors (DNMTi), histone methyltransferase inhibitors, histone deacetylase (HDAC) inhibitors (HDACi) and bromodomain and extra-terminal (BET) inhibitors (BETi) among others.[1] Despite the clinical efficacy of epigenetic drugs in hematological malignancies, chromatin-acting therapeutic strategies such as HDAC inhibition in solid tumors have so far been challenging.[2]

Pancreatic ductal adenocarcinoma (PDAC) is the most common and lethal form of pancreatic cancer. It is now the fourth leading cause of cancer death in men and women. Due to late diagnosis and metastasis, most patients with PDAC undergo conventional chemotherapy and obtain improved albeit limited benefits from intensified and toxic chemotherapy regimens, inevitably leading to secondary resistance.[3] In 2015, we reported a promising epigenetic-based therapeutic strategy for PDAC that combined BET and HDAC inhibitors.[4] We have now generated a dual inhibitor simultaneously targeting BET and HDAC proteins. Compared to combination therapies of two or more drugs, multitarget drugs may achieve the same goal but utilize a single compound. The potential advantages of dual targeting are a linked pharmacokinetic profile, reduced risk of drug-drug interactions and simplified dosing scheduling. Here, we present the design and synthesis of dual BET/HDAC inhibitors, resulting in the identification of the potent dual inhibitor TW9. Importantly, we examined its biological effects in PDAC tumor cell lines, showing its potency as a novel chromatin-targeting approach for future clinical development for treatment of PDAC.

What's new?

Preclinical evidence suggests effectiveness of the combined inhibition of bromodomain and extra-terminal (BET) and histone deacetylase (HDAC) proteins in pancreatic ductal adenocarcinoma (PDAC). However, toxicity, scheduling, and drug-drug interactions are common challenges in combined therapy. Here, the authors developed a novel dual inhibitor, TW9, simultaneously targeting BET and HDAC proteins. TW9 showed high potency in suppressing tumor growth in PDAC. Furthermore, optimized scheduling of TW9 improved the efficacy of the chemotherapeutic agent gemcitabine. The results demonstrate the potential of a dual chromatin-targeting strategy in the treatment of PDAC and provide a rationale for further development of multi-target inhibitors.

2 | MATERIALS AND METHODS

2.1 | Synthetic procedures

Synthetic routes for inhibitors 1 (TW9), 2 (TW12) and 3 (TW22) are described in detail in the Supporting Information.

2.2 | Cell culture and reagents

Pancreatic ductal adenocarcinoma cell lines (MIA PaCa-2 [RRID:CVCL_0428], PaTu 8988t [RRID:CVCL_1847], HPAC [RRID:CVCL_3517], DAN-G [RRID:CVCL_0243], PANC-1 [RRID:CVCL_0480]) and HEK293T [RRID:CVCL_0045] were obtained from ATCC and cultured in Dulbecco's Modified Eagle Medium (DMEM) containing 10% FBS, 25 mM glucose, 4 mM L-glutamine, 1 mM sodium pyruvate and 1% penicillin-streptomycin. Nut midline carcinoma cell line HCC2429 (RRID: CVCL_5132) was a gift from Lead Discovery Center GmbH (Dortmund, Germany) and was cultured in RPMI1640 medium containing 10% FBS, 2 mM L-glutamine and 1% penicillin-streptomycin. All cell lines were free of mycoplasma contamination. Cell lines (MIA PaCa-2, PaTu 8988t, HPAC, DAN-G, PANC-1) were authenticated using Multiplex human Cell line Authentication Test (MCA) by Multiplexion GmbH and cell lines HCC2429 were authenticated using short tandem repeat (STR) profiling within the last 3 years. HEK293T was only used for overexpressing nanoLUC fusion constructs. (+)-JQ1, CI994 and gemcitabine were purchased from Biomol, Selleck Chemicals and Biozol Diagnostica Vertrieb, respectively. (+)-JQ1, CI994 and gemcitabine were dissolved in DMSO as 10 mM stocks.

2.3 | Protein expression, purification and crystallography

The first two bromodomains of BRD4, BRD4(1) and BRD4(2), were each expressed in *Escherichia coli* as His-tagged proteins and were

purified by nickel-affinity and gel-filtration chromatography as described.[5] After the final gel filtration step on a Superdex-75 column in 10 mM HEPES, pH 7.5, 150 mM NaCl, 0.5 mM TCEP and 5% glycerol, the protein was concentrated to 10 mg/mL, flash-frozen in liquid nitrogen and stored at −80°C. For setting up co-crystallization trials, aliquots of the purified BRD4(1) domain were mixed with a 50 mM stock solution of TW9, TW12 or TW22 in DMSO to give a final compound concentration 1.5 mM. Crystals were grown at 4°C via the sitting drop vapor diffusion technique using a mosquito crystallization robot (TTP Labtech, Royston UK). For TW9 and TW12, crystals for data collection were grown by mixing 130 nL of protein/ligand solution with 70 nL of reservoir solution containing 24% PEG 3350, 0.1 M sodium formate, 15% ethylene glycol and 0.1 M bis-Tris-propane pH 7.3. BRD4(1) crystals in complex with TW22 were grown by mixing 100 nL of the protein/ligand solution with the same volume of reservoir solution consisting of 24% PEG 3350, 0.2 M sodium formate, 15% ethylene glycol and 0.1 M bis-Tris-propane pH 7.9. Crystals were cryoprotected with mother liquor supplemented with 20% ethylene glycol and flash-frozen in liquid nitrogen. X-ray data sets were collected at 100 K at the ESRF Grenoble, France (beamline ID30B). The diffraction data were integrated with the program XDS[6] and scaled with AIMLESS,[7] which is implemented in the CCP4 package.[8] The structures were solved by difference Fourier analysis in PHENIX[9] using PDB entry 3MXF as a starting model with initial rigid-body refinement. The structural models were then refined using iterative cycles of manual model building with COOT[10] and refinement in PHENIX. Dictionary files for the TW9, TW12 and TW22 ligands were generated using the Grade Web Server (http://grade.globalphasing.org). There was excellent electron density for the (+)-JQ1 moiety in all three structures. For TW9 and TW12, there was however not sufficient electron density to unambiguously model the solvent-exposed HDACi moiety. The disordered parts of the ligands were therefore deleted in the final model. In contrast, the HDACi moiety of TW22 was well resolved due to interaction with a symmetry-related molecule. Data collection and refinement statistics are listed in Table S1. Structural figures were prepared using PyMOL (www.pymol.org).

2.4 | Isothermal titration calorimetry

ITC measurements were performed using a Nano ITC microcalorimeter (TA Instruments, New Castle, Pennsylvania). All experiments were carried out at 15°C in ITC buffer (10 mM HEPES, pH 7.5, 150 mM NaCl, 0.5 mM TCEP and 5% glycerol). The microsyringe was loaded with the protein solution (50-150 μM protein) and titrated into an 8 to 15 μM compound solution in ITC buffer while stirring at 350 rpm. The titrations were started with an initial injection of 4 μL followed by 24 identical injections of 8 μL, at a rate of 0.5 μL/sec and a spacing of 200 seconds between injections. The heat of dilution was determined by independent titrations (protein into buffer) and was subtracted from the experimental data. Data were processed using the NanoAnalyze software (Version 3.5.0) supplied with the instrument. A single binding site model was employed.

2.5 | XTT cell viability assay

XTT cell viability assays were performed as described,[11] following the XTT kit manufacturer's instructions. Briefly, HEK293T cells were seeded into flat-bottomed 96-well plates 24 hours before the addition of test compound at a density of 2.5×10^5 cells/mL (25 000 cells/well). Then, 100 μL of test compound was added at a concentration range from 10 μM to 170 pM as final concentrations and incubated for 24 hours. For XTT measurement, 50 μL of a solution containing XTT (Sigma) and phenazine monosulfate (Sigma) were added to give a final concentration of 300 μg/mL and 10 μM, respectively, and the reaction was incubated for 30 minutes before measuring absorbance at 475 nm (specific signal) and 660 nm (nonspecific signal). The signal was background-corrected using the following formula: specific absorbance = A_{475nm}(test) − A_{475nm}(blank) − A_{660nm}(test).

2.6 | NanoBRET target engagement intracellular assay

NanoBRET target engagement assays were performed following published protocols.[12,13] Briefly, plasmids for full-length HDAC1 and BRD4 as well as the isolated bromodomains of BRD4 containing either a C-terminal (HDAC1) or an N-terminal (BRD4) placement of NanoLuc were obtained from the manufacturer (Promega, Madison, Wisconsin). To lower intracellular expression levels of the reporter fusion, the NanoLuc/kinase fusion constructs were diluted into transfection carrier DNA (pGEM3ZF-, Promega) at a mass ratio of 1:10 prior to forming FuGENE HD complexes according to the manufacturer's instructions. DNA:FuGENE complexes were formed at a ratio of 1:3 (μg DNA/μL FuGENE). One part of transfection complex solution was then mixed with 20 parts (v/v) of HEK293T cells suspended at a density of 2×10^5/mL in DMEM (Gibco) + 10% FBS (GE Healthcare, Chicago, Illinois), seeded into T75 flasks and allowed to express for 20 hours. For target engagement, the corresponding HDAC1- or BRD4-transfected cells were added and reseeded at a density of 2×10^5/mL after trypsinization and resuspension in Opti-MEM without phenol red (Life Technologies, Carlsbad, California). Serially diluted test compound and NanoBRET HDAC (Promega cat. N2140) or BRD (Promega cat. N2130) tracer were pipetted (Echo 555 Acoustic Dispenser) into white 384-well plates (Greiner 781 207). The system was allowed to equilibrate for 2 hours at 37°C/5% CO_2 prior to BRET measurements. To measure BRET, NanoBRET NanoGlo substrate + extracellular NanoLuc inhibitor (Promega) were added according to the manufacturer's protocol, and filtered luminescence was measured on a PHERAstar FSX plate reader (BMG Labtech) equipped with a luminescence filter module (450 nm [donor] and 610 nm [acceptor]).

2.7 | Fluorogenic HDAC assay

The fluorogenic HDAC assay was performed according to the manufacturer's instructions (BPS Bioscience, Cat. # 50033). Briefly,

fluorogenic HDAC substrate, test inhibitor and HDAC2 protein were mixed sequentially and incubated at 37°C for 30 minutes. Then, HDAC Assay Developer was added and incubated at room temperature for 15 minutes. The fluorescence values were measured using a Spark Multimode Microplate Reader (Tecan). The wavelengths for excitation and emission were 360 nm (bandwidth 35 nm) and 465 nm (bandwidth 35 nm), respectively.

2.8 | CellTiter Glo cell viability assay

The assay was performed according to the manufacturer's instructions (Promega, G7571). Briefly, inhibitors were preprinted in 96-well plates (Corning, Corning, New York). Then, 100 μL of cell suspension was added to the wells and cultured for indicated time periods. Then, 100 μL of diluted CellTiter-Glo Reagent (1:4 with PBS) was added to the wells. Plates were shaken for 2 minutes and incubated for another 10 minutes at room temperature in the dark. Luminescent signals were read by the Tecan Spark Multimode Microplate Reader. The values of luminescent signals were normalized to the DMSO control wells.

2.9 | Immunoblot analysis

Cell lysates were prepared in RIPA buffer (9806S, Cell Signaling Technology [CST]) containing protease inhibitor cocktail (Roche). Cell lysates were separated on SDS-polyacrylamide gels, transferred to nitrocellulose membranes with Trans-Blot Turbo Transfer System (Bio-Rad, Hercules, California) and incubated with antibodies dissolved in TBS containing 5% BSA and Tween 20 (0.1%). The following primary antibodies were used: rabbit anti-MYC (9402, CST), rabbit anti-β-actin (ab8227, Abcam, Eugene, Oregon), rabbit anti-cleaved Caspase-3 (Asp175; 5A1E; 9664, CST), rabbit anti-Caspase-3 (9662, CST), rabbit anti-acetyl-histone H3 (Lys9/Lys14; 9677, CST), mouse anti-p21 (F5) (6246, Santa Cruz), mouse anti-involucrin (i9018, Sigma-Aldrich, St. Louis, Missouri), rabbit anti-phospho-CHK1 (Ser345) (2341, CST). Primary antibodies were recognized by a peroxidase-coupled secondary antibody (Jackson, Bar Harbor, Maine) and signals were detected by chemiluminescence (ThermoFisher, Waltham, Massachusetts).

2.10 | RNA extraction and quantitative RT-PCR analysis

Total RNA was isolated using Maxwell RSC simplyRNA Cells Kit (Promega) according to the manufacturer's protocol. cDNA was synthesized using PrimeScript Reverse Transcriptase (TaKaRa, Kusatsu, Japan). cDNA was amplified using LightCycler 480 SYBR Green I Master (Roche Diagnostics, Indianapolis, Indiana) and the amplicon was detected by SYBR Green I using LightCycler 480 instrument (Roche). PCR conditions were 5 minutes at 95°C, followed by 45 cycles of 95°C for 10 seconds, 59°C for 10 seconds and 72°C for 20 seconds. The relative gene expression levels were normalized to GUSB or GAPDH and calculated using the $2^{-\Delta\Delta Ct}$ method. The primer sequences are given in Table S2.

2.11 | Crystal violet staining for colony formation assay

Attached cells were rinsed once with PBS and fixed with ice-cold methanol for 10 minutes. Fixed cells were then stained by crystal violet solution (containing 0.1% crystal violet and 25% methanol) for 30 minutes. Cells were rinsed twice with H_2O and dried overnight.

2.12 | Cell proliferation assay

MIA PaCa-2 cells (1200 cells/well) were seeded in 12-well plates (Corning). On the days of measurement, whole-well images were captured and cell confluence was analyzed by NYONE Image Cytometer (Synentec, Elmshorn, Germany).

2.13 | Cell-cycle analysis

The attached and floating cells were harvested and fixed in 70% ethanol at 4°C overnight. On the day of measurement, cells were washed once with PBS and incubated in PBS containing 0.5 mg/mL RNase A at 37°C for 30 minutes. Then, 30 μg/mL propidium iodide was added immediately before the measurement. The cellular DNA contents were analyzed by the Guava Easycyto System.

2.14 | Global gene expression profiles

Microarray using HumanHT-12 v4 Expression BeadChip (Illumina, Inc., San Diego, California) was performed by the Genomics & Proteomics Core Facility at the German Cancer Research Center in Heidelberg following the manufacturer's instructions. Raw data were normalized based on the quantile method. Hierarchical clustering of differentially expressed genes was performed using Partek Genomics Suite 7.0.

2.15 | Kaplan-Meier survival analysis

The analysis was performed using the human protein atlas data set,[14] which contains a pancreatic cancer patient cohort (n = 176). The FPKMs (number Fragments Per Kilobase of exon per Million reads) were used for quantification of expression of *FOSL1* gene. The cohort was stratified into two expression groups with the FPKM cut-off that yields the lowest P score. The correlation between the expression levels of *FOSL1* and patient survival was examined by Kaplan-Meier survival estimator.

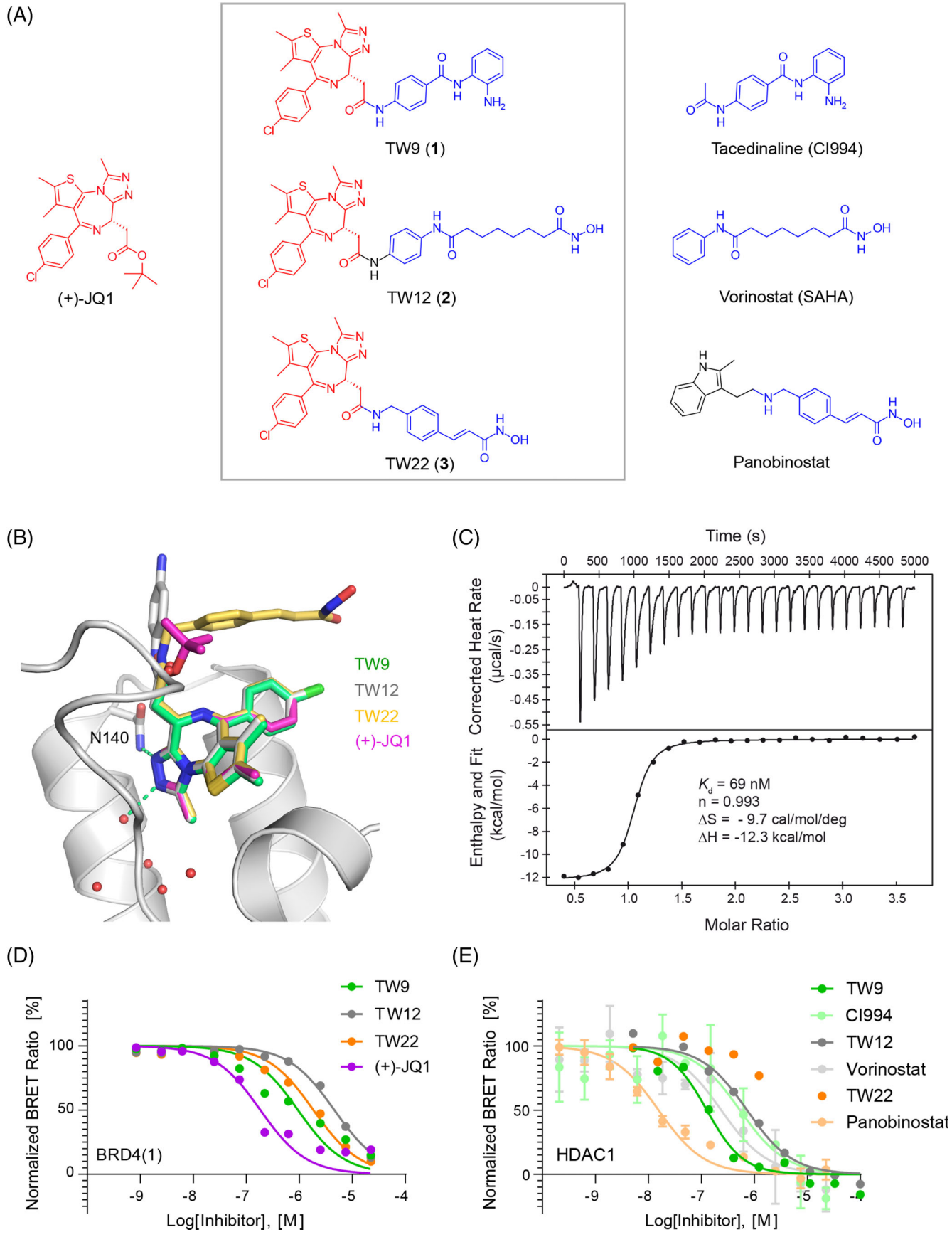

FIGURE 1 Legend on next page.

TABLE 1 Binding of dual inhibitors to BRD4 bromodomains

	In vitro K_d (μM) ITC		*In cellulo* IC_{50} (μM) NanoBRET		
Compound	BRD4(1)	BRD4(2)	BRD4(1)	BRD4(2)	FL-BRD4
TW9	0.069 ± 0.009	0.231 ± 0.031	0.72 ± 0.09	0.074 ± 0.010	0.64 ± 0.09
TW12	0.052 ± 0.006	0.088 ± 0.015	4.53 ± 0.26	11.0 ± 3.0	6.85 ± 1.04
TW22	0.021 ± 0.004	0.054 ± 0.016	1.35 ± 0.15	1.58 ± 0.54	1.43 ± 0.07
JQ1	0.051 ± 0.015	0.089 ± 0.013	0.231 ± 0.042	0.039 ± 0.008	0.104 ± 0.010

Note: Summary of the dissociation constants K_d and cellular BRD4 activity of dual inhibitors determined by isothermal titration calorimetry (ITC) and nanoBRET assays, respectively.

TABLE 2 Binding of dual inhibitors to HDAC1

Compounds	IC_{50} (μM) NanoBRET
TW9	0.29 ± 0.04
CI944	0.96 ± 0.17
TW12	1.11 ± 0.36
Vorinostat	0.52 ± 0.08
TW22	>20
Panobinostat	0.19 ± 0.10

Note: Summary of the cellular HDAC1 activity of dual inhibitors determined by nanoBRET assay.

2.16 | Bioinformatic analysis

Gene ontology (GO) analysis was performed using Gene Ontology Consortium tool (http://geneontology.org/). Gene set enrichment analysis (GSEA) was conducted using default settings on mean expression values from microarray data.[15] Sets included in the analysis ranged from 30 to 2000 genes, and gene set was used as a permutation type. For expression values for the same gene but different isoforms, values for lower expressed isoforms in control samples were disregarded. H3K27ac signal normalized to input was used to identify super-enhancers using the Ranking of Super Enhancer (ROSE) algorithm set at default settings and ignoring regions within 2500 base pairs of transcriptional start sites.[16,17] Genes associated with super-enhancers were identified by Genomic Regions Enrichment of Annotations Tool (GREAT) using default settings.[18] Publicly available datasets were used for PANC-1 [E-MTAB-7034][19] and healthy pancreas [GSM906397].[20] Mapping to the hg19 genome was performed using BOWTIE/2.2.5.[21] Bam files were generated by SAMTOOLS/1.6[22] and Bigwigs by DEEPTOOLS/2.4.0 with 200 base pair extension and ignoring the duplicates. Occupancy profiles were visualized using the Integrative Genomic Viewer.[23-25]

3 | RESULTS

3.1 | Generation of selective BET/HDAC dual inhibitors and initial in vitro characterization

For the development of dual HDAC/BET inhibitors, we synthesized three adducts that were based on the well-established BET inhibitor (+)-JQ1[5] (Figure 1A). HDAC-inhibitory activity was introduced through substitution of the tertbutyl ester by a class I selective inhibitor moiety (4-acetamido-N-[2-aminophenyl]benzamide) as present in tacedinaline (CI994), yielding the dual inhibitor TW9, as well as inhibitors for panHDAC targeting using hydroxamic acids (vorinostat and panobinostat), yielding the adducts TW12 and TW22. The synthetic routes for these inhibitors and associated analytical data are compiled in the supplemental information. The binding mode of the designed inhibitors was confirmed in crystal structures with the first bromodomain of BRD4, BRD4(1), at a resolution ranging from 1.05 to 1.25 Å (Table S1). As expected, the binding mode of the (+)-JQ1 moiety of all three adducts was essentially the same as that of the parental compound (+)-JQ1 (Figure 1B), and all key interactions with the bromodomain binding pocket were conserved, including the hydrogen bond of the triazole moiety with the highly conserved asparagine (Asn140). All HDAC moieties were solvent-accessible, suggesting that they are free to interact with HDACs even in the BET-bound state. In the case of the TW9 and TW12 complexes, the HDAC inhibitory moieties were disordered. In the structure of the TW22 complex, however, the HDAC inhibitor, which was derived from panobinostat, was visible due to stabilization by crystal contacts (Figures 1B and S1).

For initial functional evaluation, we determined the dissociation constants, K_d, of binding to the first and second bromodomain of BRD4, BRD4(1) and BRD4(2), by isothermal titration calorimetry (ITC). All three adducts (TW9, TW12 and TW22) bound to the first bromodomain, BRD4(1), with low nM affinity, resulting in K_d values of

FIGURE 1 Rational design of BET/HDAC dual inhibitors and initial characterization. A, Chemical structure of (+)-JQ1-HDACi-adducts and their parental molecules. B, Crystal structure of dual inhibitors in complex with BRD4(1). The structure of the BRD4(1)-TW9 complex is shown as a gray cartoon representation, with the TW9 ligand shown as a green stick model. Conserved structural water molecules in the binding pocket are shown as small red spheres. The binding modes of TW12, TW22 and the parental molecule (+)-JQ1 are superimposed, showing that the binding mode of the (+)-JQ1 moiety is essentially the same in all four structures. The solvent-exposed HDACi moieties of TW9 and TW12 were largely disordered, and the corresponding atoms were deleted from the final model, whereas the HDACi moiety of TW22 was stabilized via interaction with a symmetry-related molecule in the crystal. C, Isothermal titration calorimetry experiment of TW9 binding to BRD4(1). The upper panel shows the raw binding heats for each injection, and in the lower panel, normalized binding isotherms are shown. D, Cellular BRD4(1)-targeting activity of dual inhibitors measured by NanoBRET assay. E, Cellular HDAC1-targeting activity of dual inhibitors measured by NanoBRET assay [Color figure can be viewed at wileyonlinelibrary.com]

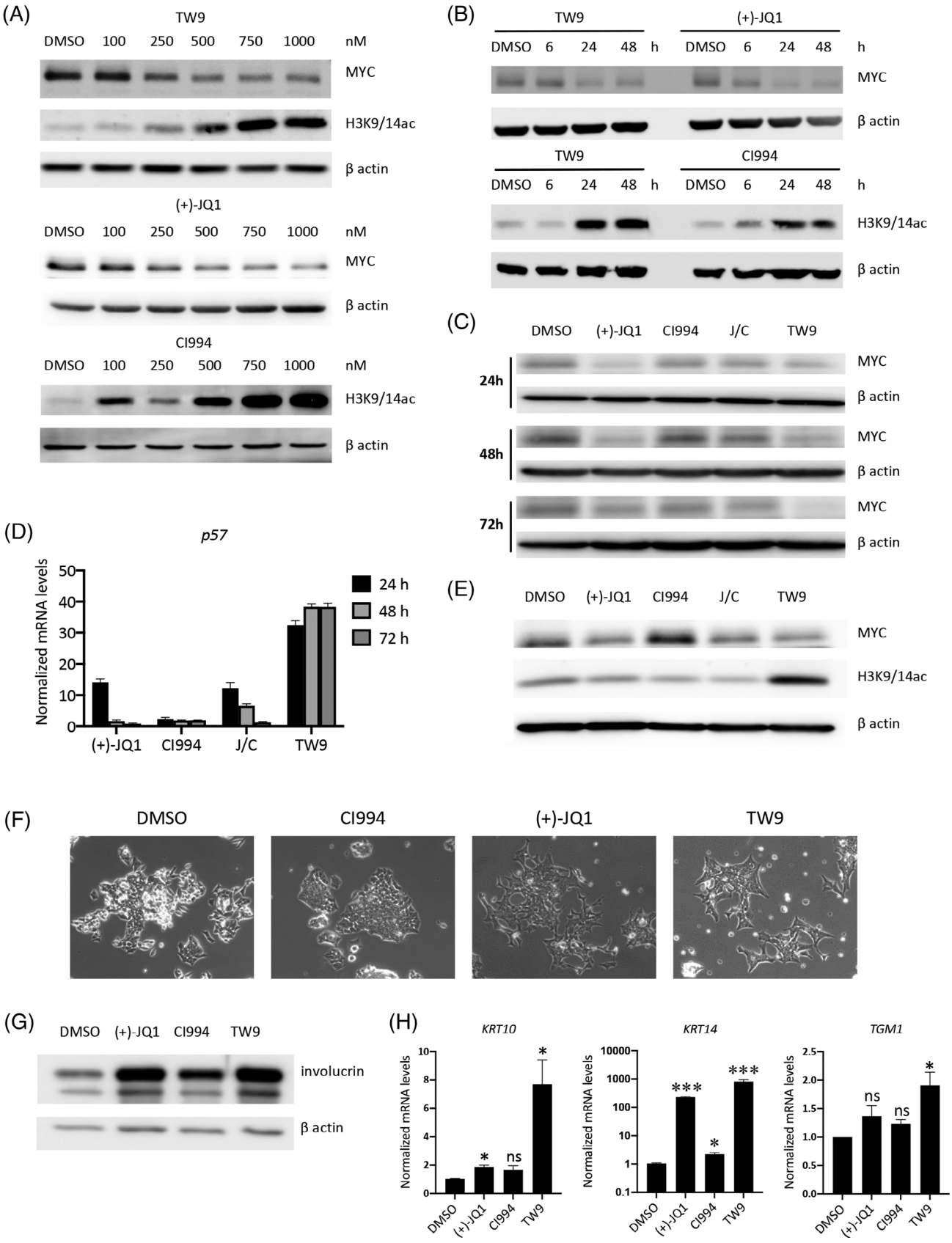

FIGURE 2 Legend on next page.

69, 52 and 21 nM, respectively, which was in the range of the K_d value determined for the parental molecule (+)-JQ1 (51 nM; Table 1). A representative ITC experiment for TW9 is shown in Figure 1C. K_d values for BRD4(1) were all slightly higher, ranging from 230 nM for TW9 to 54 nM for TW22, which again was similar to the K_d of (+)-JQ1. In summary, the ITC measurements demonstrated excellent BET binding activity of our dual inhibitors, indicating that introduction of the HDAC-inhibitor moiety did not significantly alter affinities for the two bromodomains present in BRD4.

Next, we tested the cellular BRD4 activity of the synthesized adducts using nanoBRET assays (Table 1 and Figure 1D). All nanoBRET experiments were carried out in HEK293T cells under non-toxic conditions (Figure S2). TW9 showed the best BRD4-targeting activity, with an IC_{50} value of around 700 nM for BRD4(1) (Figure 1D). The affinity of TW12 and TW22 for BRD4(1) in cells was notably weaker, with IC_{50} values of 5.5 and 12 μM, respectively. A similar trend was observed for the cellular affinity of our dual inhibitors to BRD4(2). Notably, TW9 had a 10 times higher affinity for BRD4(2) than for BRD4(1), with an IC_{50} value of 74 vs 720 nM, and bound BRD4(2) more than 20 times more strongly than did TW12 and TW22 (Table 1). Comparison of the ITC and nanoBRET data suggests that the drastically reduced potency of TW12 and TW22 in cells compared to (+)-JQ1 was most likely due to reduced cellular uptake rather than differences in intrinsic binding affinity. We also measured cellular K_ds for the full-length BRD4 protein, FL-BRD4. In all cases, the measured apparent binding constants were as expected between the values obtained for the two isolated bromodomains (Table 1).

After confirming the BRD4-targeting activity, we performed further NanoBRET assays to determine the cellular activity of our compounds against HDACs, the second target protein class of our dual inhibitors (Table 2 and Figure 1E). TW9 was a potent inhibitor of HDAC1 with an IC_{50} value in cells of about 300 nM. As such, it was more potent than the parental HDAC inhibitor CI994, which had an IC_{50} of around 1 μM under the same conditions. TW12 was less potent than TW9 in targeting HDAC1, and TW22 displayed an even lower potency in cells with an IC_{50} > 20 μM, corresponding to a potency more than three orders of magnitude lower compared to its parental compound panobinostat (Table 2). We also performed a cell-free fluorogenic HDAC assay, which showed that TW9 and CI994 inhibited HDAC2 activity to a similar degree, with IC_{50} values of 2.5 and 1.7 μM, respectively (Figure S3). Based on the above results, we chose TW9 as the most potent BET/HDAC dual inhibitor for further characterization in cancer cells.

3.2 | TW9 preserves both BETi and HDACi activities in cancer cells

Both *MYC* and *HEXIM1* are often used as readout biomarkers of BET inhibitor activity in cancer cells, while acetylated histone H3 is used as a direct readout for HDAC inhibitor activity. Expression analysis by RT-PCR showed prompt (6 hours) down-regulation of *MYC* and upregulation of *HEXIM1* by TW9 to similar levels as (+)-JQ1 (Figure S4A). Immunoblot analysis showed that MYC and histone H3 acetylated at lysines 9 and 14 were regulated in a dose- and time-dependent manner by TW9 (Figure 2A,B), comparable to (+)-JQ1 and CI994, respectively. Consistent with the nanoBRET assays for HDAC-targeting activity of TW9 (Table 2 and Figure 1E), histone H3 acetylation at lysine 9 and 14 was enhanced by TW9 at a much higher level, compared to the parental HDAC inhibitor CI994 (Figures 2B and S4B). Intriguingly, when we treated cells with a higher dose (4 μM) of TW9, we observed a more sustained suppression of MYC and induction of p57, a target previously identified as being regulated by combined BET/HDAC inhibition,[4] indicating more sustained BETi activity of TW9 (Figure 2C,D). In contrast, we did not observe the sustained BETi activity with 1 μM TW9 (Figure S2C,D). In addition, we performed washout experiments (1 day on and 2 days off) and still observed enhanced histone H3 acetylation at lysine 9 and 14 in both 1 and 4 μM TW9-treated samples on day three (Figures 2E andS2E).

We next implemented immunoblot analysis of MYC and histone H3 acetylated at lysines 9 and 14 in cells treated with TW12 and TW22. Both ligands down-regulated MYC to the same degree as (+)-JQ1, indicating preserved (+)-JQ1 activity (Figure S4F). However, TW12 and TW22 failed to accumulate acetylated histone H3, indicating decreased activity of the HDAC-inhibitor moiety (Figure S4F).

3.3 | TW9 induces squamous differentiation in NUT midline carcinomas

We next assessed the biological activity of TW9. NUT midline carcinoma (NMC) is a poorly differentiated squamous cell carcinoma defined by chromosomal rearrangement of the *NUT* gene, most often fused with *BRD4*. A previous study showed that BRD4-NUT inhibition by (+)-JQ1 was able to induce squamous differentiation.[5] Thus, we tested if TW9 could also induce differentiation in the NMC cell line HCC2429.[26] Like (+)-JQ1, TW9 provoked a differentiation phenotype in HCC2429, featuring cell spreading, flattening, and striking spindle

FIGURE 2 TW9 preserves both BETi and HDACi activities, and induces squamous differentiation in NMC. A, Dose-dependent manner of MYC and H3K9/14 ac protein levels by immunoblot. PaTu 8988t cells were treated with the indicated doses of inhibitors for 48 hours. B, Time-dependent manner of MYC and H3K9/14 ac protein levels by immunoblot. PaTu 8988t cells were treated with 1 μM indicated inhibitors and harvested at the indicated time points. C and D, Time-course analysis of MYC protein levels by immunoblot (C) and *p57* mRNA levels by quantitative RT-PCR (D). PaTu 8988t cells were treated with 4 μM indicated inhibitors and harvested at the indicated time points. Mean ± SEM from three independent experiments. E, Immunoblot analysis of drug washout experiment in PaTu 8988 t cells treated with 4 μM indicated inhibitors (24 hours on and 48 hours off). F, Morphological changes of NMC cell line HCC2429 treated with 500 nM indicated inhibitors for 48 hours. G, Immunoblot analysis of involucrin, a differentiation marker, in HCC2429 cells treated with 500 nM indicated inhibitors for 72 hours. H, Quantitative RT-PCR analysis of canonical squamous tissue genes (*KRT10*, *KRT14* and *TGM1*) in HCC2429 cells treated with 500 nM indicated inhibitors for 72 hours. Mean ± SEM from three independent experiments, $^{***}P \le .001$, $^{**}P \le .01$, $^{*}P \le .05$; n.s., not significant

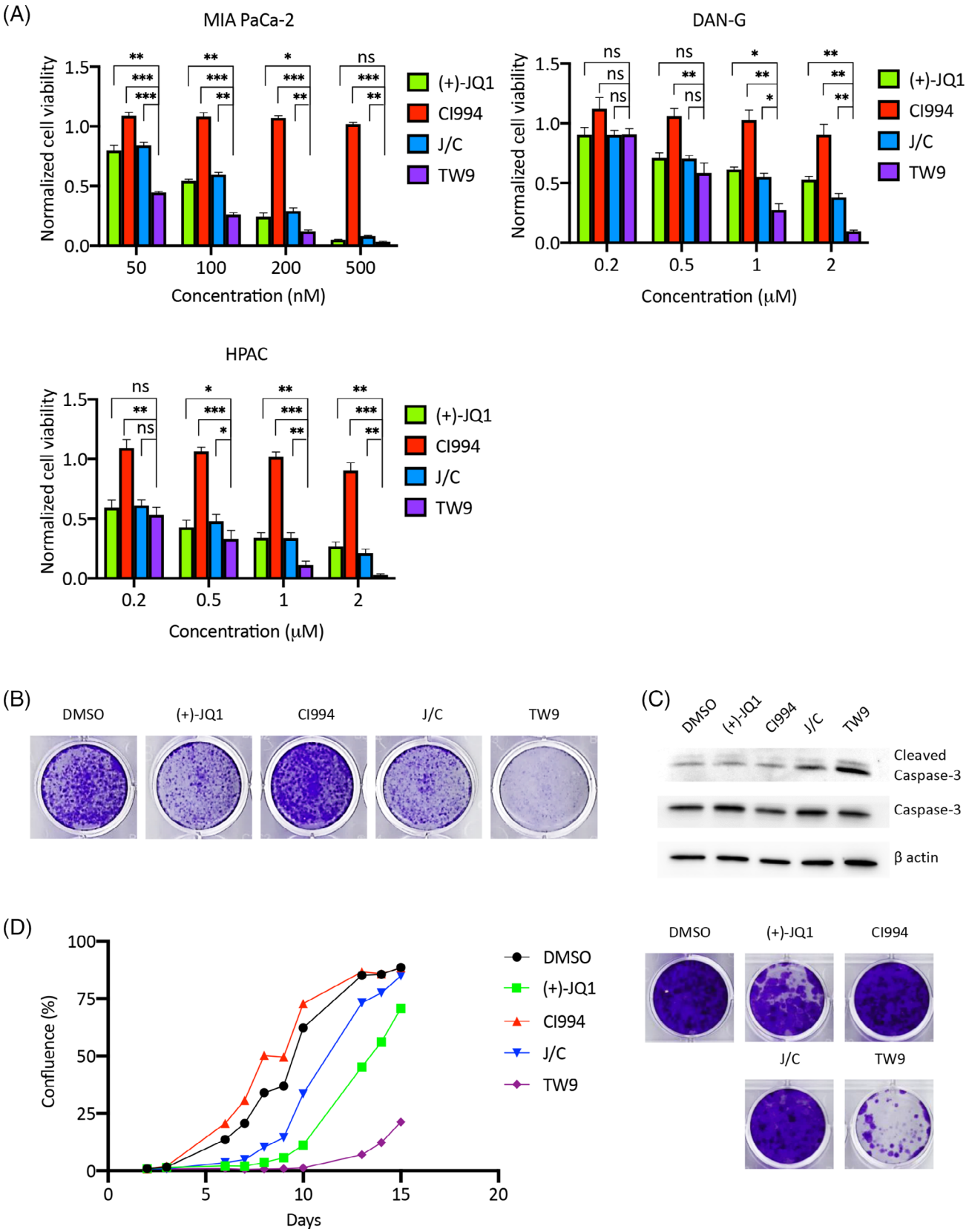

FIGURE 3 TW9 is a more potent antiproliferation molecule than its parental molecules or combinations thereof. A, CellTiter Glo cell viability assay using four different PDAC cell lines treated with different doses of the indicated inhibitors for 5 days. Mean ± SEM from three independent experiments, ***$P \leq .001$, **$P \leq .01$, *$P \leq .05$; n.s., not significant. B, Colony formation assay of MIA PaCa-2 cells treated with 50 nM indicated inhibitors for 5 days. C, Immunoblot analysis of cleaved caspase-3 in MIA PaCa-2 cells treated with 50 nM indicated inhibitors for 3 days. D, Cell confluence measurement of MIA PaCa-2 cells after treatment of 1 μM indicated inhibitors for 24 hours by NYONE image cytometry (left). At end time point, cells were stained for colony formation assay (right) [Color figure can be viewed at wileyonlinelibrary.com]

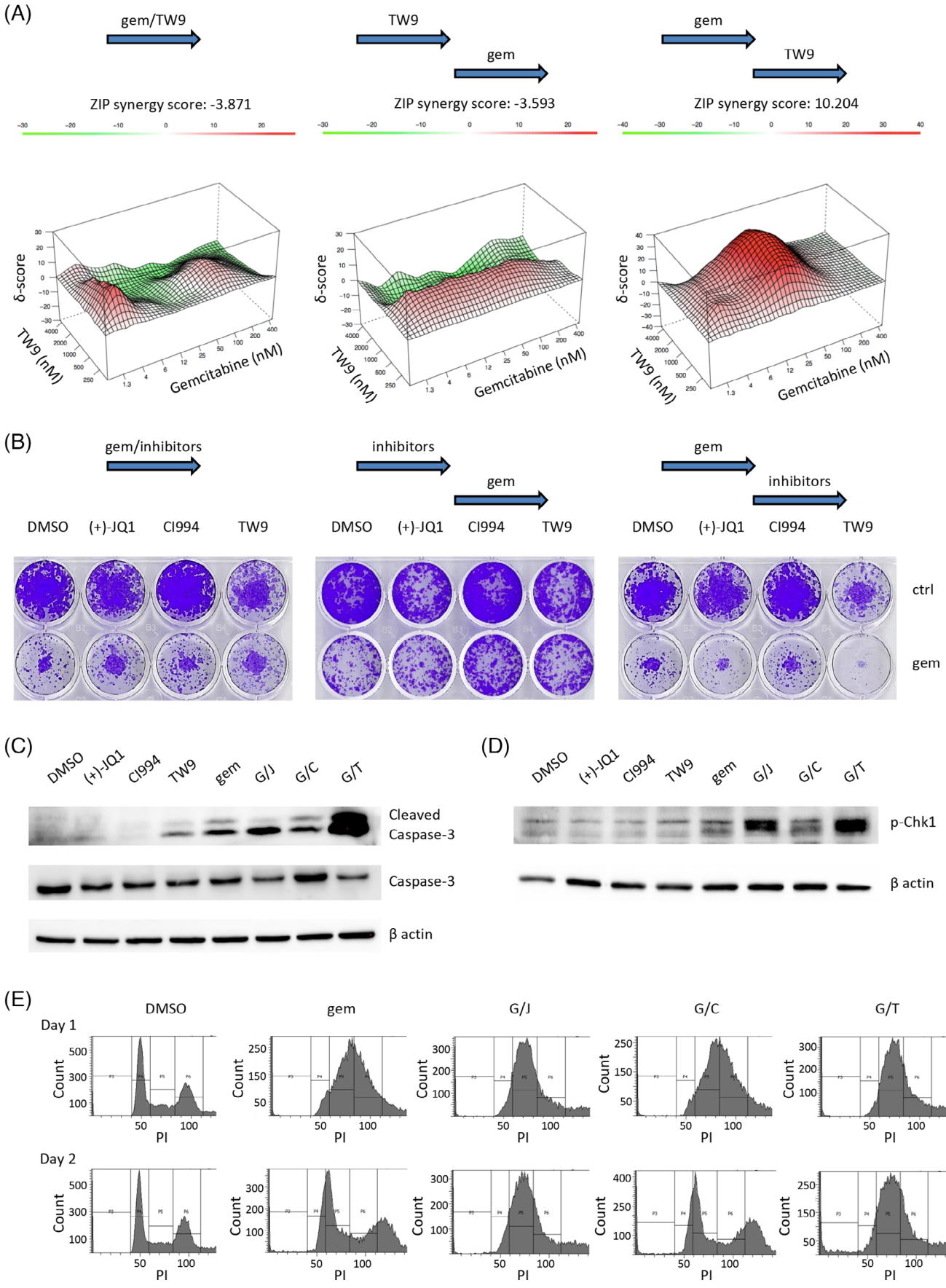

FIGURE 4 Legend on next page.

morphology (Figure 2F). Furthermore, TW9 induced gene expression of Involucrin, a differentiation marker, to a similar level as (+)-JQ1 (Figure 2G). Expression analysis of three canonical squamous tissue genes by RT-PCR showed marked (>700-fold) induction of *KRT14* and modest induction of *KRT10* (6-fold) and *TGM1* (2-fold) by TW9 (Figure 2H). Notably, TW9 was significantly more efficient than (+)-JQ1 in inducing the expression of each of these genes.

3.4 | TW9 is more potent in suppressing growth of pancreatic cancer cells than its parental molecules

We next performed cell viability assays in a panel of PDAC cell lines (MIA PaCa-2, DAN-G and HPAC) and observed that TW9 decreased cell survival in a dose-dependent manner (Figure 3A). Furthermore, TW9 showed a more potent effect on cell survival when compared to (+)-JQ1, CI994 alone or the combination of (+)-JQ1 and CI994. Colony formation assay also showed that TW9 was more potent in suppressing cell growth (Figures 3B and S5A,B). Immunoblot analysis clearly showed that TW9 treatment led to increased expression of cleaved caspase 3, consistent with apoptotic cell death (Figure 3C).

In current clinical trials, single-agent BET inhibition is challenged by limited effectiveness, toxicity issues and still largely unknown optimal scheduling strategies.[27] To evaluate alternative scheduling strategies early on, we evaluated the long-term effects on cell survival of TW9 when administered only once for a time period of 24 hours. Compared to single-agent or combination treatment with (+)-JQ1 and CI994, TW9 had more sustained effects on suppressing cell growth, and cells started to grow much later (Day 10; Figure 3D, left panel). Colony formation assay at the end time point also showed much fewer colonies formed by TW9-treated cells (Figure 3D, right panel). Next, we applied a schedule for TW9 (1 day on and 6 days off for 3 cycles), which further prolonged the suppressive effects (Figure S5C). Thus, dosing of TW9 may be reduced with ongoing tumor-suppressive activity.

3.5 | Sequential administration of gemcitabine and TW9 shows synergistic effects

Gemcitabine is a standard-of-care chemotherapeutic agent in the treatment of PDAC. Previous combination of gemcitabine with the HDAC inhibitor CI994 resulted in increased toxicity and no beneficial effect of this combination in a phase II clinical trial.[28] Thus, we evaluated the efficacy of combining TW9 and gemcitabine using different scheduling routes. Gemcitabine and TW9 were administered either at the same time or sequentially. Serial dilutions of each compound were combined, and the effect on the viability of HPAC cells was measured by cell viability assay. A synergistic effect between gemcitabine and TW9 was observed and most prominent when gemcitabine was given 24 hours before TW9 (G1T2 schedule, Figures 4A,B and S6A). Cleaved caspase 3 staining induced by G1T2 schedule supports highly increased apoptosis (Figure 4C). After the same schedule, we also performed synergistic test for JQ1/CI994 when combined with gemcitabine (Figure S6B). The ZIP score (8.96) of JQ1/CI994 is lower than that of TW9 (10.20), proving benefits of TW9 as a dual inhibitor. Strikingly, simultaneous or sequential administration of TW9 first followed by gemcitabine showed no combinatorial benefits or even detrimental effects in colony formation (Figures 4B and S7A), indicating that TW9 may reduce sensitivity to gemcitabine in these schedules. Consistent with previous reports, we found that (+)-JQ1 as well as TW9 induced accumulation of the cell-cycle regulator p21 (Figure S7B), which led to G1 arrest (Figure S7C). We assumed that the attenuated S-phase entry by (+)-JQ1 or TW9 inhibited gemcitabine incorporation into replicating DNA. To support this hypothesis, we found that simultaneous administration of gemcitabine and (+)-JQ1 or TW9 retained more cells in G1 phase compared to gemcitabine treatment alone, which induced early S-phase arrest (Figure S7D).

As known, gemcitabine induces acute replication stress as indicated by the induction of phospho-CHK1, and withdrawal of gemcitabine releases cells from such stress (Figure S7E). Simultaneous treatment of TW9 followed by gemcitabine largely prevented cells from replication stress induced by gemcitabine (Figure S7F). However, G1T2 scheduling enhanced the gemcitabine-induced replication stress (Figure 4D). Withdrawal of gemcitabine relieved replication stress and cells returned to normal cell-cycle distribution (Figure 4E). However, after the G1T2 schedule, cells maintained S-phase arrest after drug withdrawal (Figure 4E). In summary, G1T2 scheduling showed the most prominent synergistic effects by augmenting gemcitabine-induced replication stress and apoptosis.

3.6 | TW9 blocks cell-cycle progression through super enhancer-associated transcription factor FOSL1

To explore the molecular mechanisms elicited by TW9, transcriptomic profiling was performed in the established PDAC cell line PANC-1.

FIGURE 4 Administration of TW9 with chemotherapy. A, Combination response to TW9 and gemcitabine for HPAC cells treated with three administration schedules: (1) simultaneous administration of gemcitabine and TW9 for 24 hours and incubation for another 4 days; (2) Sequential administration of TW9 and gemcitabine (each for 24 hours) and incubation for another 3 days; (3) Sequential administration of gemcitabine and TW9 (each for 24 hours) and incubation for another 3 days. CellTiter Glo cell viability assay was performed to measure cell viabilities for all the indicated dose combinations. Synergy effects were evaluated using SynergyFinder (synergyfinder.fimm.fi).[39] The ZIP synergy score is averaged over all the dose combination cells. B, Colony formation assay for HPAC cells treated with different administration schedules indicated above. Here, 10 nM gemcitabine and 2 μM individual inhibitors were used. C and D, HPAC cells were sequentially treated with 10 nM gemcitabine and 2 μM individual inhibitors. Then, inhibitors were removed, and cells were cultured for another 1 day for immunoblot analysis of cleaved caspase-3 and phospho-CHK1. E, HPAC cells were treated as above and harvested at 24 and 48 hours after removal of inhibitors for cell-cycle analysis [Color figure can be viewed at wileyonlinelibrary.com]

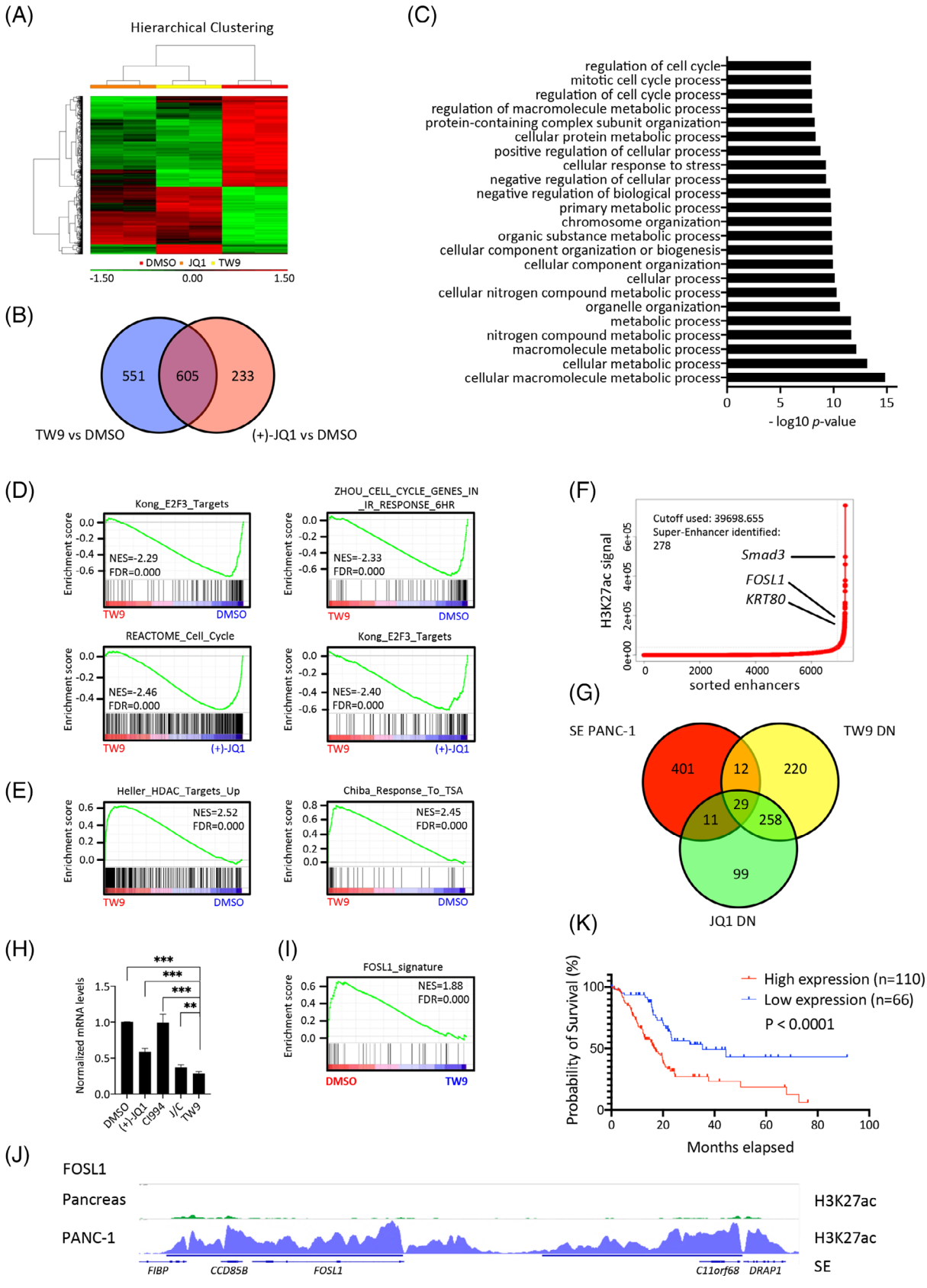

FIGURE 5 Legend on next page.

Hierarchical clustering of the differentially expressed genes by either TW9 or (+)-JQ1 revealed distinct gene expression profiles between TW9 and (+)-JQ1-treated samples (Figure 5A). Around 70% of the differentially expressed genes by (+)-JQ1 were also deregulated by TW9 (Figure 5B), indicating that TW9 largely recapitulates the activity of (+)-JQ1. To obtain a deeper insight into the gene expression patterns altered by TW9, we performed gene ontology (GO) analysis. Interestingly, the genes downregulated by TW9 were mainly associated with metabolic processes, cellular component organization and cell-cycle-related processes (Figure 5C). Gene set enrichment analysis (GSEA) also revealed that the significantly enriched pathways involved in cell cycle progression were downregulated by TW9 in comparison with DMSO or (+)-JQ1 treatment (Figure 5D). Furthermore, HDAC inhibition was among the most significantly enriched pathways in TW9-treated samples (Figure 5E), indicating that TW9 also recapitulates the activity of CI994.

Further, we aimed to identify TW9-regulated master transcriptional regulators (TFs) that control cell-cycle progression. Previous studies suggested that master TFs could be driven by super-enhancers (SEs).[29] We thus performed ChIP-seq using H3K27ac to identify the genomic enhancer landscape. Bioinformatic analysis of the genome-wide occupancy of H3K27ac resulted in the identification of 453 SEs in PANC-1 cells (Figure 5F). We next analyzed SE-associated gene expression of TW9- or (+)-JQ1-treated cells compared to controls. Venn diagram analysis shows that 41 TW9-downregulated genes were associated with SEs (Figure 5G). Compared to (+)-JQ1 treatment, 12 SE-associated genes were identified to be selectively targeted by TW9, including the transcription factor FOSL1. FOSL1 has previously been linked to KRAS-associated mitotic progression.[30] To confirm the downregulation of FOSL1 by TW9, we performed RT-PCR and found that FOSL1 was indeed downregulated by TW9 to a larger extent, compared to (+)-JQ1, CI994 and combined treatment (Figure 5H). Moreover, GSEA analysis revealed that FOSL1 targets[30] were significantly downregulated by TW9 (Figure 5I), implying that TW9 dysregulated the transcriptional program of FOSL1. Consistent with the elevated levels of FOSL1 in PDAC,[30] we found SEs around the FOSL1 gene locus in PANC-1 cells but not in healthy pancreas (Figure 5J), supporting the notion that cancer cells establish super-enhancers at oncogenes during tumor pathogenesis.[29] Statistical analysis of a pancreatic cancer cohort from the Human Protein Atlas data set[14] revealed that FOSL1 is a prognostic marker and that high FOSL1 expression levels are unfavorable for patient survival (Figure 5K). These results suggest that the antiproliferative phenotype observed in TW9-treated cells may involve targeting of the FOSL1-regulated mitotic machinery.

4 | DISCUSSION

Current drug discovery remains widely dominated by the "one gene, one drug, one disease" paradigm. However, this paradigm has been continuously challenged in terms of redundant functions and alternative complex compensatory signaling patterns that are especially common in cancer. Thus, the biological rationale is compelling to consider multitarget approaches over single-target strategies. Conventional multitarget approaches include drug combinations, where it is difficult to achieve equitable pharmacokinetics and biodistribution. To solve this issue, our study aimed at a single compound that has multiple inhibitory activities. We designed and synthesized ligands by conjugating two distinct pharmacophores (BETi and HDACi).

In our study, the ligand TW9 contains (+)-JQ1 and CI994 moieties showing dual inhibitory activities against BRD4 and HDAC proteins. Here we show that TW9 is a more potent BET/HDAC dual inhibitor than the combination of the parent molecules (+)-JQ1 and CI994, showing promising antiproliferative activities in vitro in PDAC. Similar dual BET/HDAC inhibitors have been reported in previous studies.[31-34] In a recent study,[34] a dual BET/HDAC inhibitor (compound 13a) with a structure very similar to TW9 was reported. The difference is that the *ortho*-aminoanilide in the CI994 moiety is replaced with hydroxamic acid in compound 13a. This modification makes compound 13a a potent pan-HDAC inhibitor, whereas our TW9 is a class I selective HDAC inhibitor. Both probes (TW9 and compound 13a) are valuable and complementary tools in cellular context-dependent studies. However, as a potential limitation, TW9 represents an adduct of two inhibitory moieties, resulting in a dual inhibitor with a relatively large molecular weight. In future studies, we aim to integrate both functionalities in a single inhibitor in a manner that will reduce molecular weight. Such dual inhibitors with BET activity have already been reported for BET-kinase combinations by us and other research groups.[35-38]

Intriguingly, we observed that TW9 had enhanced and more sustained HDAC-inhibiting effects when assessing histone H3 acetylation at lysines 9 and 14 by western blot analysis and in the drug washout experiment, suggesting that the CI994 moiety on TW9 has a longer residence time on its targets. While this needs further

FIGURE 5 TW9 blocks cell-cycle progression through super-enhancer associated transcription factor FOSL1. A and B, Hierarchical clustering (A) and Venn diagram analysis (B) of the differentially expressed genes in PANC-1 cells treated with 1 μM TW9 or (+)-JQ1 for 24 hours compared to DMSO treatment. Each treatment was done in duplicate. C, Gene ontology analysis of TW9-downregulated genes. D and E, GSEA plots comparing the enrichment of cell cycle-related pathways (D) and HDAC inhibition signature (E). F, Enhancers in PANC-1 ranked based on H3K27ac signal intensity using the ROSE algorithm defining 453 super-enhancers. G, Venn diagram analysis identifying TW9-specific super-enhancers. H, Quantitative RT-PCR analysis of *FOSL1* gene in PANC-1 cells treated with 1 μM indicated inhibitors for 24 hours. Mean ± SEM from six independent experiments, $^{***}P \leq .001$, $^{**}P \leq .01$, $^{*}P \leq .05$; n.s., not significant. I, GSEA plot comparing the enrichment of FOSL1 signature. J, H3K27ac occupancy profiles at the *FOSL1* gene in PANC-1 and the healthy counterpart. K, Kaplan-Meier plot showing the survival of pancreatic cancer patients stratified by *FOSL1* mRNA expression levels [Color figure can be viewed at wileyonlinelibrary.com]

characterization, it may explain why TW9 has more prolonged growth-inhibitory effects in the long-term proliferation assay.

Chemotherapy remains the standard-of-care treatment for PDAC patients with limited long-term effectiveness. In our study, we addressed if TW9 administration could improve the efficacy of gemcitabine, a well-tolerated chemotherapeutic agent with limited single-drug activity in PDAC. Strikingly, different schedules for administration yielded highly different results. We found that the cell-cycle arrest by cotreatment with TW9 interferes with the incorporation of gemcitabine into newly synthesized DNA and suppresses gemcitabine-induced replication stress. In contrast, TW9 treatment after gemcitabine administration sustains gemcitabine-induced S-phase arrest and replication stress. This result may explain why we did not previously observe synergism between (+)-JQ1 and gemcitabine in a PDAC mouse model, in which twice daily treatment of (+)-JQ1 plus a Q3Dx4 schedule (every third day for four cycles) for gemcitabine administration was applied.[4]

Previous studies implied that super-enhancers play key roles in the control of cell identity and disease.[29] In our study, we discovered that PANC-1 tumor cells display super-enhancers at the oncogene FOSL1. This led to the activation of a FOSL1 downstream transcriptional program that supports tumor cell proliferation. The transcriptional addiction of tumor cells to certain regulators of gene expression provides opportunities for therapeutic interventions in cancer. Along this line, we propose a model where TW9, by targeting the super enhancer-associated *FOSL1* gene, may counteract the dysregulated transcriptional program and inhibit tumor cell proliferation.

As a proof of concept, our data support future efforts at developing chromatin-acting multitarget drugs harboring potential benefits for clinical application: a linked pharmacokinetic profile, reduced risk of drug-drug interactions and simplified dosing schedules. We are now designing a second generation of BET/HDAC dual inhibitors that integrate the two pharmacophores to achieve a lower molecular weight and more drug-like physicochemical properties.

ACKNOWLEDGEMENTS

We are grateful to Nicola Bielefeld, Konstantinos Savvatakis, Anna Bazarna and Mihaela Keller for technical assistance. We also thank the staff at ESRF Grenoble beamline ID30B and Deep Chatterjee for assistance during X-ray data collection. J. T. S., S. K., S. J. and S. A. H. are supported by the German Cancer Aid (grant no. 70112505; PIPAC consortium). J. T. S. and S. K. are further supported by the German Cancer Consortium (DKTK). J. T. S. receives also funding from the Deutsche Forschungsgemeinschaft (DFG) through grant SI1549/3-1 (Clinical Research Unit KFO337) and Collaborative Research Center SFB824 (project C4). A. C. J. is funded by the German Research Foundation (DFG) grant JO 1473/1-1. S. K. is grateful for support by the SGC, a registered charity (number 1097737) that receives funds from AbbVie, Bayer Pharma AG, Boehringer Ingelheim, Canada Foundation for Innovation, Eshelman Institute for Innovation, Genome Canada, Innovative Medicines Initiative (EU/EFPIA), Janssen, Merck KGaA Darmstadt Germany, MSD, Novartis Pharma AG, Ontario Ministry of Economic Development and Innovation, Pfizer, São Paulo Research Foundation-FAPESP, Takeda, and Wellcome [106 169/ZZ14/Z].

CONFLICT OF INTEREST

No conflicts of interest are disclosed by the authors.

DATA ACCESSIBILITY

Coordinates and structure factors of the complexes of BRD4(1) with the inhibitors TW9, TW12, and TW22 have been deposited in the Protein Data Bank (PDB). Accession codes: 6YQN, 6YQO, and 6YQP. The Human Protein Atlas data set for Kaplan-Meier survival analysis is available via https://www.proteinatlas.org.

ORCID

Swetlana Ladigan https://orcid.org/0000-0003-1923-4096
Jens T. Siveke https://orcid.org/0000-0002-8772-4778

REFERENCES

1. Jones PA, Issa JP, Baylin S. Targeting the cancer epigenome for therapy. *Nat Rev Genet*. 2016;17(10):630-641.
2. Li Y, Seto E. HDACs and HDAC inhibitors in cancer development and therapy. *Cold Spring Harb Perspect Med*. 2016;6(10):a026831.
3. Conroy T, Desseigne F, Ychou M, et al. FOLFIRINOX versus gemcitabine for metastatic pancreatic cancer. *N Engl J Med*. 2011;364(19):1817-1825.
4. Mazur PK, Herner A, Mello SS, et al. Combined inhibition of BET family proteins and histone deacetylases as a potential epigenetics-based therapy for pancreatic ductal adenocarcinoma. *Nat Med*. 2015;21(10):1163-1171.
5. Filippakopoulos P, Qi J, Picaud S, et al. Selective inhibition of BET bromodomains. *Nature*. 2010;468(7327):1067-1073.
6. Kabsch W. Xds. *Acta Crystallogr D Biol Crystallogr*. 2010;66(Pt 2):125-132.
7. Evans PR. An introduction to data reduction: space-group determination, scaling and intensity statistics. *Acta Crystallogr D Biol Crystallogr*. 2011;67(Pt 4):282-292.
8. Winn MD, Ballard CC, Cowtan KD, et al. Overview of the CCP4 suite and current developments. *Acta Crystallogr D Biol Crystallogr*. 2011;67(Pt 4):235-242.
9. Adams PD, Afonine PV, Bunkoczi G, et al. PHENIX: a comprehensive python-based system for macromolecular structure solution. *Acta Crystallogr D Biol Crystallogr*. 2010;66(Pt 2):213-221.
10. Emsley P, Lohkamp B, Scott WG, Cowtan K. Features and development of Coot. *Acta Crystallogr D Biol Crystallogr*. 2010;66(Pt 4):486-501.
11. Roehm NW, Rodgers GH, Hatfield SM, Glasebrook AL. An improved colorimetric assay for cell proliferation and viability utilizing the tetrazolium salt XTT. *J Immunol Methods*. 1991;142(2):257-265.
12. Machleidt T, Woodroofe CC, Schwinn MK, et al. NanoBRET—A novel BRET platform for the analysis of protein-protein interactions. *ACS Chem Biol*. 2015;10(8):1797-1804.
13. Asquith CRM, Berger BT, Wan J, et al. SGC-GAK-1: a chemical probe for Cyclin G associated kinase (GAK). *J Med Chem*. 2019;62(5):2830-2836.
14. Uhlen M, Zhang C, Lee S, et al. A pathology atlas of the human cancer transcriptome. *Science*. 2017;357(6352):eaan2507.
15. Subramanian A, Tamayo P, Mootha VK, et al. Gene set enrichment analysis: a knowledge-based approach for interpreting genome-wide expression profiles. *Proc Natl Acad Sci USA*. 2005;102(43):15545-15550.

16. Loven J, Hoke HA, Lin CY, et al. Selective inhibition of tumor oncogenes by disruption of super-enhancers. *Cell*. 2013;153(2):320-334.
17. Whyte WA, Orlando DA, Hnisz D, et al. Master transcription factors and mediator establish super-enhancers at key cell identity genes. *Cell*. 2013;153(2):307-319.
18. McLean CY, Bristor D, Hiller M, et al. GREAT improves functional interpretation of cis-regulatory regions. *Nat Biotechnol*. 2010;28(5):495-501.
19. Hamdan FH, Johnsen SA. DeltaNp63-dependent super enhancers define molecular identity in pancreatic cancer by an interconnected transcription factor network. *Proc Natl Acad Sci USA*. 2018;115(52):E12343-E12352.
20. Bernstein BE, Stamatoyannopoulos JA, Costello JF, et al. The NIH roadmap Epigenomics mapping consortium. *Nat Biotechnol*. 2010;28(10):1045-1048.
21. Langmead B, Salzberg SL. Fast gapped-read alignment with Bowtie 2. *Nat Methods*. 2012;9(4):357-359.
22. Li H, Handsaker B, Wysoker A, et al. The sequence alignment/map format and SAMtools. *Bioinformatics (Oxford, England)*. 2009;25(16):2078-2079.
23. Ramirez F, Dundar F, Diehl S, et al. deepTools: a flexible platform for exploring deep-sequencing data. *Nucleic Acids Research*. 2014;42(Web Server Issue):W187-W191.
24. Robinson JT, Thorvaldsdottir H, Winckler W, et al. Integrative genomics viewer. *Nat Biotechnol*. 2011;29(1):24-26.
25. Thorvaldsdottir H, Robinson JT, Mesirov JP. Integrative genomics viewer (IGV): high-performance genomics data visualization and exploration. *Brief Bioinform*. 2013;14(2):178-192.
26. Wang R, Liu W, Helfer CM, et al. Activation of SOX2 expression by BRD4-NUT oncogenic fusion drives neoplastic transformation in NUT midline carcinoma. *Cancer Res*. 2014;74(12):3332-3343.
27. Alqahtani A, Choucair K, Ashraf M, et al. Bromodomain and extra-terminal motif inhibitors: a review of preclinical and clinical advances in cancer therapy. *Future Sci OA*. 2019;5(3):FSO372.
28. Richards DA, Boehm KA, Waterhouse DM, et al. Gemcitabine plus CI-994 offers no advantage over gemcitabine alone in the treatment of patients with advanced pancreatic cancer: results of a phase II randomized, double-blind, placebo-controlled, multicenter study. *Ann Oncol*. 2006;17(7):1096-1102.
29. Hnisz D, Abraham BJ, Lee TI, et al. Super-enhancers in the control of cell identity and disease. *Cell*. 2013;155(4):934-947.
30. Vallejo A, Perurena N, Guruceaga E, et al. An integrative approach unveils FOSL1 as an oncogene vulnerability in KRAS-driven lung and pancreatic cancer. *Nat Commun*. 2017;8:14294.
31. Atkinson SJ, Soden PE, Angell DC, et al. The structure based design of dual HDAC/BET inhibitors as novel epigenetic probes. *Med Chem Commun*. 2014;5(3):342-351.
32. Zhang Z, Hou S, Chen H, et al. Targeting epigenetic reader and eraser: rational design, synthesis and in vitro evaluation of dimethylisoxazoles derivatives as BRD4/HDAC dual inhibitors. *Bioorg Med Chem Lett*. 2016;26(12):2931-2935.
33. Amemiya S, Yamaguchi T, Hashimoto Y, Noguchi-Yachide T. Synthesis and evaluation of novel dual BRD4/HDAC inhibitors. *Bioorg Med Chem*. 2017;25(14):3677-3684.
34. He S, Dong G, Li Y, Wu S, Wang W, Sheng C. Potent dual BET/HDAC inhibitors for efficient treatment of pancreatic cancer. *Angew Chem Int Ed Engl*. 2020;59(8):3028-3032.
35. Ciceri P, Muller S, O'Mahony A, et al. Dual kinase-bromodomain inhibitors for rationally designed polypharmacology. *Nat Chem Biol*. 2014;10(4):305-312.
36. Andrews FH, Singh AR, Joshi S, et al. Dual-activity PI3K-BRD4 inhibitor for the orthogonal inhibition of MYC to block tumor growth and metastasis. *Proc Natl Acad Sci USA*. 2017;114(7):E1072-E1080.
37. Liu S, Yosief HO, Dai L, et al. Structure-guided design and development of potent and selective dual Bromodomain 4 (BRD4)/polo-like kinase 1 (PLK1) inhibitors. *J Med Chem*. 2018;61(17):7785-7795.
38. Watts E, Heidenreich D, Tucker E, et al. Designing dual inhibitors of anaplastic lymphoma kinase (ALK) and Bromodomain-4 (BRD4) by tuning kinase selectivity. *J Med Chem*. 2019;62(5):2618-2637.
39. Ianevski A, He L, Aittokallio T, et al. SynergyFinder: a web application for analyzing drug combination dose-response matrix data. *Bioinformatics (Oxford, England)*. 2017;33(15):2413-2415.

SUPPORTING INFORMATION

Additional supporting information may be found online in the Supporting Information section at the end of this article.

How to cite this article: Zhang X, Zegar T, Weiser T, et al. Characterization of a dual BET/HDAC inhibitor for treatment of pancreatic ductal adenocarcinoma. *Int. J. Cancer*. 2020;147:2847–2861. https://doi.org/10.1002/ijc.33137